LAWRENCE
LIVERMORE
NATIONAL
LABORATORY

UCRL-JRNL-208501

Desorption/Ionization Fluence Thresholds and Improved Mass Spectral Consistency Measured Using a Flattop Laser Profile in the Bioaerosol Mass Spectrometry of Single Bacillus Endospores

P. T. Steele, A. Srivastava, M. E. Pitesky, D. P. Fergenson, H. J. Tobias, E. E. Gard, M. Frank

December 10, 2004

Analytical Chemistry

Desorption/Ionization Fluence Thresholds and Improved Mass Spectral Consistency Measured Using a Flattop Laser Profile in the Bioaerosol Mass Spectrometry of Single *Bacillus* Endospores

Paul T. Steele, Abneesh Srivastava, Maurice E. Pitesky, David P. Fergenson, Herbert J. Tobias, Eric E. Gard and Matthias Frank[*]

Lawrence Livermore National Laboratory, 7000 East Ave., L-211, Livermore, CA 94550

Abstract

Bioaerosol mass spectrometry (BAMS) is being developed to analyze and identify biological aerosols in real-time. Mass spectra of individual *Bacillus* endospores were measured here with a bipolar aerosol time-of-flight mass spectrometer in which molecular desorption and ionization were produced using a single laser pulse from a Q-switched, frequency-quadrupled Nd:YAG laser that was modified to have an approximately flattop profile. The flattened laser profile allowed the minimum fluence required to desorb and ionize significant numbers of ions from single aerosol particles to be determined. For *Bacillus* spores this threshold had a mean value of approximately 1 nJ/μm^2 (0.1 J/cm^2). Thresholds for individual spores, however, could apparently deviate by 20% or more from the mean. Threshold distributions for clumps of MS2 bacteriophage and bovine serum albumin were subsequently determined. Finally, the flattened profile was observed to increase the reproducibility of single spore mass spectra. This is consistent with the general conclusions of our earlier paper on the fluence

[*] E-mail: frank1@llnl.gov Telephone: 925-423-5068 Fax: 925-424-2778

dependence of single spore mass spectra and is particularly significant because it is expected to enable more robust differentiation and identification of single bioaerosol particles.

Introduction

Single-particle aerosol mass spectrometry is an established technique for the rapid chemical analysis of individual aerosol particles[1] and has been implemented in a number of forms [2-7]. In typical systems, aerosol particles are sucked directly from the atmosphere into vacuum through a series of small orifices[8]. As the particles approach the ion source region of the mass spectrometer, they cross and scatter light from two CW laser beams separated by a known distance[9]. The timing of the two bursts of scattered light created by each "tracked" particle reveals the speed, location and size of the particle. This information then enables the firing of a high-intensity laser such that the resulting laser pulse desorbs and ionizes molecules from the tracked particle just as it reaches the center of the ion source region. The full spectrum of ions is then measured using a time-of-flight mass spectrometer.

This ability to rapidly analyze individual particles is clearly of value for the rapid detection of aerosolized biological warfare agents so long as agent particles can be made to produce mass spectra that are distinct from the spectra of harmless background particles. The pattern of ions formed is determined by the properties of the laser pulse and the particle. Given the importance of speed and throughput, it is generally impractical to modify the particle properties (coating the particles with a MALDI matrix may be an exception[10-12]). As a result, it is critical that the properties of the laser pulses used for desorption and ionization be carefully chosen. In one of our previous papers[13], it was shown that the laser fluence has a significant effect upon the mass spectra produced by *Bacillus* spores. Consequently the profile of the desorption/ionization (DI) laser must affect the reproducibility of single spore mass spectra. A simple observation of interest here is that as the fluence is lowered, a threshold is reached at which no detectable spectra are generated.

The fluence thresholds for different types of particles are needed to optimize and predict the performance of future BAMS systems. They are also relevant to other types of instruments. Several bioaerosol detectors measure UV fluorescence from biological particles[14-19]. More intense UV excitation

generally leads to more intense fluorescence[20], which is beneficial, but if the excitation is too intense the aerosol particles will be damaged potentially interfering with more selective methods of subsequent analysis. For such instruments, the fluence thresholds determined here serve as absolute upper limits on the excitation fluences that should be used (some damage is likely at fluences well below these levels however).

In a BAMS system, consistency of mass spectra is also clearly important if identification and differentiation of similar particle types is to be robust. Consequently, the laser profile is an important parameter to optimize. The range of fluences produced by any non-uniform laser pulse will cause imperfectly focused aerosol particles to absorb varying amounts of energy since successive particles can interact with different portions of the laser profile. Variations in the energy absorbed cause variations in the spectra produced. The importance of a flat laser profile was recently and directly demonstrated for aerosol particles composed of 2,4-dihydroxybenzoic acid[21]. Here we flattened our laser's profile using a different, simpler method and demonstrate that the variability of spectra from complex biological particles, specifically spores, is reduced. Quantifying this reduction in a meaningful manner is not trivial. Special care was taken, in particular, to choose appropriate Gaussian and flattop profiles so that resulting data sets could be fairly compared.

It should be noted that the instrument used here is intended for proof-of-concept laboratory experiments and not for use as an actual biological agent detector. Sampling efficiencies and other system parameters that are relevant for a fielded detector will not be discussed here since these do not affect the conclusions drawn from the experiments described.

Experimental Section

Instrumental layout

The basic instrumental layout is shown in Figure 1 and was described previously[13]. Samples were aerosolized using a Collison nebulizer[22, 23]. The initially wet bioaerosols were passed through a diffusion drier, containing activated silica gel desiccant, and then directed through copper tubing to the aerosol mass spectrometer inlet. The mass spectra ultimately obtained were saved to disk for later analysis.

Sample Preparation

Bacillus atrophaeus (*B.at.*), formerly *B. globigii*, is frequently used as a surrogate for *Bacillus anthracis* (*B.a.*) by the Department of Defense. For the present experiments, *B.at.* cells (ATCC #9372, Dugway Proving Ground, Dugway, UT) were grown to mid-log phase in tryptone yeast extract broth (¼×TY) and then aliquoted into 75 ml of fresh broth in a 1:25 dilution. The cells sporulated in a shaker incubator at 32°C until approximately 90% were refractile (3-4 days). Phase contrast microscopy and spore staining confirmed that spores were in fact present. The spores were then harvested by centrifugation at 8000 g for 12 minutes, and washed in cold double-distilled water. After three washes the spores were reconstituted in double distilled-water at concentrations of approximately 10^6 spores/ml (as determined using a Petroff-Hauser counting chamber).

Using a similar procedure, *B.at.* and *Bacillus thuringiensis* (*B.t.*) spores were also prepared in resuspension (rs) media. In the case of *B.at.*, this second growth medium was employed to reveal some of the effects that the preparation routine can have on the observed mass spectra. *B.t.* (ATCC No. 16494) was included as a surrogate for naturally occurring particle types that might easily be misidentified as *B.a.* (or *B.at.* in the current experiments).

MS2 bacteriophage were used as a crude surrogate for viral agents such as smallpox. The sample was obtained from the ATCC (No. 15597-B1) and seemed to contain significant impurities from buffers and salts. Bovine serum albumin (BSA) served as a rough surrogate for toxins such as ricin. It was obtained from Sigma (Fraction V, ≥96%).

Profile Modification of DI Laser

As in our previous paper[13], the DI laser was a Q-switched, frequency-quadrupled Nd:YAG laser (Ultra CFR, Big Sky Laser Technologies, Inc.) that produced pulses with a wavelength of 266 nm, a pulse length of ~6 ns and a roughly Gaussian beam profile. The Ultra used here, however, had a new, more efficient, fourth harmonic crystal that produced higher pulse energies (>7 mJ/pulse at the laser

head) and reduced high-spatial-frequency profile variations. In further contrast to the earlier experiments, the laser beam profile was "flattopped" using extracavity optics.

A number of methods have been used to produce flattop laser profiles[21, 24-27]. Since the Ultra provided more energy than needed, a relatively simple method (see Figure 1) was used here to flatten the profile at the cost of a significant fraction of the laser pulse energy. Just outside the laser head, a half-wave plate followed by a UV thin film polarizer allowed the pulse energy to be continuously adjusted (by rotation of the waveplate) while the Ultra ran at full power. Running the laser at full power was critical since this mode of operation produced a profile with a relatively flat central portion, minimized the pulse-to-pulse energy fluctuations (~1.4% standard deviation) and also minimized the timing jitter between the Q-switch trigger and the actual laser pulse.

After the polarizer, a harmonic separator reflected the 266 nm pulses, while unwanted 532 nm light was transmitted and dumped. The low intensity wings around the central flat portion of each 266 nm pulse were then clipped by a 1 mm circular aperture. The clipped pulses were reflected off two mirrors (used for beam alignment), passed through a lens (f≈130 mm) and window, and finally delivered to the center of the ion source region of the mass spectrometer. The distances between the aperture, lens and target plane were carefully set such that a properly focused, one-third sized (320 μm diameter) image of the uniform profile at the aperture was obtained at the target plane. (The target plane is defined here as the plane normal to the laser beam that contains the axis of the particle stream, where particles are most likely to interact with the laser.) To verify that the focusing was correct, a second lens imaged the laser profile at the target plane (or optionally nearby planes) onto a Coherent LaserCam IIID camera with a BIP-12F UV profiling attachment located outside the mass spectrometer. Figure 2a shows an image of the flattened profile.

The fluence distribution plots (or modified fluence histograms) introduced previously[13] are a useful tool to quantify the flatness of the "flattop" profiles. The distributions are not commonly presented so their generation will be briefly described. Multiple images of the flattened laser beam profile at the target plane were acquired at a fixed laser setting. For each image, the absolute fluence was calculated

for each pixel and a histogram of the values was produced. The number of pixels falling in each fluence bin was multiplied by the area per pixel (~19 μm^2) to find the total area in the laser cross-section falling in the fluence range represented by the bin. Histograms from 21 images were then averaged and scaled to produce the final distributions, examples of which are shown in Figure 3. The distributions show the range of fluences that an individual aerosol particle may encounter at a given laser setting. The distributions include the effects of shot-to-shot energy and profile variations but are primarily shaped by the remaining inhomogeneities in the mean laser profile.

Since the diameter of the focused particle stream is significantly larger than the diameter of the laser profile, the aerosol particle distribution is expected to be relatively uniform across the laser profile. In such a situation, the average area in the beam at a given fluence should be proportional to the probability of a particle interacting with that fluence. In the case of Figure 3a, for example, a particle is likely to encounter either a fluence near zero (which is unlikely to produce a spectrum) or a fluence between 2 and 3 $nJ/\mu m^2$. The new profiles are clearly not perfectly flat (a finite range of non-zero fluences exists), but they are vastly superior to the original "Gaussian" profiles.

Results and Discussion

Fluence Thresholds

The most extensive set of mass spectral data was obtained for *B.at.* (¼×TY) spores. Its collection and the analysis required to determine the threshold fluence are thus described here first. The collection and processing of data from the other samples was virtually identical, so only the results and a few important differences will be mentioned. It should be noted that MALDI experiments indicate that there may be a fluence threshold for the desorption of neutral material below the threshold for ionization[28, 29]. Neutral material cannot be detected in the present instrument, so the thresholds reported here entail both desorption and ionization.

The laser energy was initially set to a value (~430 μJ) where the average fluence (~5 $nJ/\mu m^2$) was well above the expected threshold fluence. From this starting point, the energy was stepped downward

until the hit rate fell nearly to zero and then stepped back up (retracing the earlier steps) to the starting energy. (The hit rate is defined as the ratio of the number of particles that produce spectra to the number of particles tracked.) Each time the laser energy was lowered, the spores absorbed less energy on average and fewer of them were able to produce enough free ions to generate a spectrum. Even so, each time the laser energy was changed, ~300 spectra were collected, except at the very lowest energy where only a few spectra were collected because of time constraints. Figure 4 shows average mass spectra collected at several different laser energies. The general appearance of the spectra is similar to those shown in previous papers[13, 30, 31] where most of the peaks have been identified. The prominence of the potassium peak at m/z=39 in the present spectra may be related in part to the fact that it is the only element likely to be encountered with an ionization potential less than the energy of a single 266nm photon (4.34 eV versus 4.66 eV respectively).

The data points in Figure 5 show the hit rates observed as a function of energy. Error bars result from finite counting statistics. The hit rates are expected to be significantly less than unity because imperfectly focused particles can pass through both tracking lasers but pass well to either side of the ~320 μm DI laser beam. Inaccuracies in the timing system also cause the DI laser to occasionally fire at aerosol particles before (or after) they reach the proper vertical position. For the present discussion, however, the absolute magnitude of the hit rate does not matter but only relative changes.

The shape of the hit rate curve depends primarily upon the shape of the laser profile and the distribution of single spore fluence thresholds, which could be narrow or broad. (Variations in pulse energy are small enough to be safely ignored.) If the laser profile was perfectly flat and all spores had exactly the same fluence threshold, the hit rate would be zero until the laser fluence exceeded the threshold and then the hit rate would jump instantly to its maximum value and remain there. This was not observed. The influence of the imperfect profile must be taken explicitly into account; only thereafter it is possible to quantify the width of the spore threshold distribution more rigorously.

If the assumption is made, for the moment, that all the spores had the same fluence threshold and that the spores were equally likely to encounter any portion of the laser profile, the hit rate at a given laser

energy should be proportional to the area in the profile above the fluence threshold. If for example, a certain fraction of the area in the profile *A* was initially above the threshold and then the laser energy was increased such that the area above threshold doubled (to *2A*), the probability that a spore would interact with that area would also double. Consequently the observed hit rate would double. Based on the measured properties of the laser profiles it is possible to predict the expected shape of the hit rate curve in this situation. It turns out, however, that the predicted curve (not shown) is too steep by roughly a factor of two.

The most likely explanation for the additional softening of the hit rate curve (beyond that caused by the laser profile) is that different spores have at least slightly different thresholds. This is not an unreasonable hypothesis because spores are known to have a range of sizes and chemical properties. If the assumption is made that the spore population has a normal (i.e. Gaussian) distribution of thresholds characterized by a specific mean and standard deviation, these two parameters can be determined from the hit rate data by simple curve fitting. (The non-uniformities in the beam are still taken into account as well.) The conclusion of the fitting procedure is that *B.at.* spores grown in ¼×TY media have a distribution of DI fluence thresholds with a mean of 1.0 nJ/μm^2 and a standard deviation of 0.23 nJ/μm^2. (Note that 0.23 nJ/μm^2 is not the uncertainty in the mean but rather the width of the actual distribution.) As shown in Figure 5, this model reproduces the observed hit rate data well.

The width of the fluence threshold distribution cannot be quantitatively predicted on the basis of currently measured spore properties, but its magnitude does seem compatible with the scale of size and compositional inhomogeneities expected in the spore population. For a typical set of data, the mean aerodynamic diameter of analyzed spores was roughly ~1.0 μm with a standard deviation of 0.1 μm. This finite size range leads to a range of absorbed energies. Consider two spores: one with a diameter approximately one standard deviation below the mean (0.9 μm) and another with a diameter approximately one standard deviation above the mean (1.1 μm). The amount of energy that they would absorb (assuming a fluence of 1 nJ/μm^2, uniform composition and spherical shape) can be calculated approximately using the complex index of refraction of *B. subtilis* spores in water (n=1.550+0.0138i at

265 nm[32]) and a freely available Mie scattering program[33]. The result is that the 0.9 μm (physical) diameter spore would absorb 0.34 nJ of laser energy or 0.89 nJ/μm^3 while the 1.1 μm diameter spore would absorb 0.56 nJ or 0.80 nJ/μm^3. It is almost certain, therefore, that these spores would have different thresholds even though it is implicitly assumed that they have identical chemical compositions (i.e. the same bulk index of refraction). The fact that the chemical compositions do vary will cause additional variations in the fluence threshold. The dipicolinic acid (DPA) content of *B. subtilis* W23 spores has been observed to vary by 30%[34]. Since DPA absorbs at 266 nm, such variations must affect the amount of energy absorbed by the spore and hence the fluence threshold. The inferred magnitude of variation in fluence threshold seems physically reasonable.

As mentioned earlier, *B.at.* spores were also prepared in resuspension (rs) media. The same basic experimental procedure was repeated. *B.at.* (rs) spores were found to have a distribution of fluence thresholds with a mean of 1.0 nJ/μm^2 and a standard deviation of 0.24 nJ/μm^2. These values agree very well with the results obtained for *B.at.* (¼×TY). The *B.at.* (rs) mass spectra were also very similar to those shown for *B.at.* (¼×TY) in Figure 4. One significant difference was that the peak at m/z=+74 tended to be smaller in the spectra from spores in resuspension media. This peak is important since it helps differentiate certain *Bacillus* species[35].

Sets of data from *B.t.* spores grown in resuspension media were also collected in a similar fashion. *B.t.* spores appear to have a distribution of fluence thresholds with a mean of 1.1 nJ/μm^2 and a standard deviation of 0.3 nJ/μm^2. The *B.t.* spores have a slightly higher mean threshold than the *B.at.* spores analyzed earlier. This is probably related to the fact that the average aerodynamic diameter of the *B.t.* spores was 1.05 μm while the value for *B.at.* spores was 0.98 μm (for particles producing spectra). The threshold distribution is also broader for the *B.t.* spores. This is consistent with the observation that the *B.t.* did not sporulate as uniformly as the *B.at.* and that the *B.t.* size distribution was broader than that of *B.at.* The *B.t.* spore mass spectra were similar to those produced by *B.at.* spores but, differences in the areas of peaks at m/z=-173 (the negative sign indicates that it is a negative ion) and +74 are usually sufficient to differentiate the two species[35].

Since the two species of *Bacillus* spores have basically the same size and similar chemical compositions, it is not surprising that they have similar thresholds (~1 nJ/μm^2). Furthermore, the value of the threshold itself seems physically reasonable. Based on the complex index of refraction mentioned earlier, a 1 μm spore is expected to absorb 0.47 nJ at a fluence of 1 nJ/μm^2. The heat capacity of a spore is unknown but can be approximated very crudely using the heat capacity of tryptophan, which is 238.1 J/mol K. With a density of 1.45 g/ml [36], a spore is thus estimated to heat by ~530°C upon interaction with the laser pulse. It is interesting to note that the expected final temperature is therefore similar to the temperature of the pyrolysis tube (550°C) in the BLOCK II Chemical Biological Mass Spectrometer (CBMS)[37]. It is also of the same order of magnitude as the peak matrix surface temperature predicted in a typical UV MALDI experiment using DHB[38].

The same data collection process used for spores was repeated for clumps of MS2 virions and clumps of BSA. The size distributions of both aerosolized samples had a mean aerodynamic diameter of ~0.9 μm and a standard deviation of 0.15 μm. The quality of the BSA data was somewhat less than that for the other particle types because a low hit rate limited the amount of data that could be collected. Nonetheless, MS2 particles were observed to have a distribution of fluence thresholds with a mean of 3.2 nJ/μm^2 and a standard deviation of 0.8 nJ/μm^2. BSA particles were observed to have a distribution of fluence thresholds with a mean of 2.7 nJ/μm^2 and a standard deviation of 0.4 nJ/μm^2. It should be noted that impurities in the BSA sample seem to have had a significant effect on the observed mass spectra and may have affected the fluence threshold. The relatively high fluence thresholds for MS2 and BSA particles are hypothesized to result, at least in part, from absorption coefficients that are lower at 266 nm than those for spores, but this will have to be confirmed with future experiments (note that absorption, as opposed to the more easily measured total extinction, must be quantified).

Direct Observation of Variability Reduction with Flattop

Maximizing the consistency of spectra from individual particles is clearly advantageous for the rigorous identification of single particles. One of our previous papers[13] showed that a non-uniform laser

profile must contribute to the variations between individual mass spectra, but quantifying this affect is not trivial. Data collected with a non-uniform (e.g. Gaussian) profile can only be meaningfully compared to data collected with a flattop profile if the properties of the profiles are carefully matched. In the experiment described here, the properties of a flattop profile were precisely measured at two different average pulse energies. Matching "Gaussian" profiles were then carefully created to contain the same amount of area, at or above the fluence threshold as the matching flattop profile, and also the same amount of pulse energy in this area. To be clear, the total pulse energy was not the same, but rather the energy contained in the areas of the beam where the fluence met or exceeded the chosen threshold value. It was thus ensured that the "effective" average fluence was the same in both profiles. Note that the conditions necessary for a match depend upon the properties of the particles analyzed. *B.at.* spores were used here because of their general importance as an anthrax surrogate and because their DI fluence threshold was known.

Although the thresholds of different spores vary, a single representative value for the threshold was chosen here for the sake of simplicity. In particular, a value slightly below the mean was chosen (0.95 $nJ/\mu m^2$) since this value seemed best at reproducing the observed hit rate behavior in a model where all spores were assumed to have the same fluence threshold. Mass spectra were collected with flattop profiles using average pulse energies of 106 μJ and 147 μJ. To characterize these pulses, twenty-one images of the flattened profile at the target plane (Figure 2a) were collected and the area in each image that had a fluence greater than or equal to 0.95 $nJ/\mu m^2$ was calculated. The average of these areas was then found and converted to an "effective diameter" for convenience. (The effective diameter of an area or region is defined here as the diameter of a perfect circle with the same area.) The effective diameters of the flattop profiles were 314 μm and 320 μm, respectively. The average energies contained within the above threshold regions were 97 μJ and 136 μJ (the remainder of the energy was spread over lower fluence regions). The fluence distributions are shown in Figure 6. Notice that the two distributions are almost entirely above the 0.95 $nJ/\mu m^2$ fluence threshold and are also fairly distinct from one another.

The optical scheme used to obtain matching "Gaussian" pulses was largely identical to the one shown in Figure 1, except that the aperture was removed and the original lens was replaced and repositioned. The laser was operated at less than its maximum energy setting to produce a more Gaussian-like profile, but the waveplate and polarizer were still used to fine-tune the average pulse energy. To match the low-fluence flat profile, a laser spot with a diameter of ~330 μm (FWHM) and an average total pulse energy of 197 μJ was produced. This resulted in an above threshold region with an average effective diameter of 312 μm containing an average of 97 μJ of energy (Figure 2b). To match the high-fluence flat profile, a ~240 μm (FWHM) spot was created with a total average energy of 187 μJ. This produced an effective diameter of 318 μm and a contained energy of 138 μJ (Figure 2c). The fact that the total energy in this high-fluence Gaussian was less than the total energy in the low-fluence Gaussian is not surprising; less energy was wasted in large low-fluence wings. The fluence distributions for these profiles are also shown in Figure 6. One thousand mass spectra were obtained for each of the four profiles such that the standard deviations of the laser pulse energy were ~1.2% for the flattop profiles and ~5% for the Gaussian profiles. Compared with the range of fluences present in these pulses due to profile variations, the pulse energy fluctuations should be insignificant.

One of the more common means of determining the similarity of mass spectra is to represent them as vectors in a high-dimensional space and then calculate the angle between them[13, 21, 40]. The n^{th} element of a vector represents the area of the peaks in the associated mass spectrum near the integer mass-to-charge ratio of n (usually all peaks out to m/z=±350 are included with separate vectors for positive and negative ions). Such a calculation is computationally straightforward and often yields useful results. Nonetheless, it tends to give undue weight to large ion peaks while neglecting smaller peaks that may still be important. This shortcoming can be reduced by dividing each element of each vector by the square root of its mean value before calculating an angle. On a basic, practical level, this simply makes the big peaks smaller relative to the little peaks. In an ideal system, where fluctuations in peak areas are dominated by ion counting statistics, dividing by the square root ensures that all of the vector elements have the same standard deviation, which is desirable. The angle between normalized vectors can be

found, but as will be shown in a future paper, the geometric distance between normalized vectors is a more convenient metric to work with mathematically. Before proceeding, it is important to recognize that most of the elements in the vectors don't represent actual signal but rather chemical or electronic noise, which is not of interest. Consequently only the ten positive and ten negative vector elements with the largest mean values (based on an average of all the vectors in all data sets) were retained for the present analyses. This corresponds roughly to the number of significant peaks observed in the spectra.

For each set of data, a normalized ten-element vector (as just described) was derived for each polarity of each individual spectrum. The distance from each vector to its associated mean vector (the mean of all the same polarity vectors in the data set) was then calculated. Histograms of these normalized distances are shown in Figure 7. The root-mean-square (RMS) distance from an individual vector to its mean vector was also calculated and is labeled for each polarity of each set (this distance is the actual metric of variability). A basic interpretation of the histograms is straightforward. Identical spectra produce identical vectors and the distance between these vectors is zero, the more dissimilar the spectra, the greater the distance between them. In the case of a set of data, if all the spectra were identical, the RMS distance from an individual vector to the mean vector would be zero; the more variable the set of data, the larger the RMS distance becomes. Figure 7 shows that the flattop profiles produced less variability than their matching Gaussian profiles. This is clear from the labeled RMS distances, but it is also apparent visually for the high fluence histograms. The variability reduction is less pronounced for the low fluence profiles. This is probably related to the fact that the biggest absolute changes in mean peak areas occur at high energies (~150-300 μJ) when the pulse energy is changed (Figure 5).

Fortunately, the ~20% average reduction of the RMS distances may represent much more than a 20% increase in the number of particle types that the BAMS system can differentiate at a given confidence level. Each mean vector defines a point in 10-dimensional space. The individual vectors in a set define points that are spread about the mean point. In the ideal case, for which the normalization scheme can be rigorously developed and applied, the individual points are spread across a hypersphere centered at the mean point (ignoring correlations between peaks for the moment). Clearly if the hyperspheres from different types of particles overlap significantly, it will be difficult if not impossible to differentiate the

particle types. The number of hyperspheres that can be fit within a specific region of 10-dimensional space is proportional to the their "hypervolume". The hypervolume of a hypersphere in 10 dimensions is proportional to its radius (i.e. the RMS-distances labeled in Figure 7) raised to the tenth power. A 20% reduction in the radius corresponds to a 90% reduction in hypervolume, and this could theoretically increase the number of different particles that can be discriminated by up to a factor of 10. This may not be trivial to grasp, but the simple conclusion is that the reduction of observed variability will likely have its greatest impact when large numbers of different types of particles must be differentiated and identified.

Although the spectral variability has been reduced, it should be noted that a considerable amount of variability remains. This is presumably due to statistical processes, which are always involved in the production and detection of a finite number of ions, and natural particle variations. The statistical processes will be addressed in a future paper.

Conclusions

Different types of biological particles have different fluence thresholds. This is not surprising, but it is important because it affects the performance of the BAMS system as well as other single particle aerosol instruments. If particle fluorescence is to be analyzed, the excitation fluence will generally have to be kept below the lowest threshold of all the particle types of interest. In the case of mass spectrometry, on the other hand, the DI laser fluence must generally be kept above the highest fluence threshold of all the particle types of interest even though this may not produce optimal spectra from all particles. The choice of an optimal fluence for an actual biological agent detector will depend upon the properties of agent particles as well as background particles and also the user's requirements for speed, probability of detection and probability of false alarm; it is a topic worthy of a paper in its own right. Regardless of the fluence chosen, however, increased mass spectral consistency will always be desirable. A flattened laser profile represents an important improvement in this area and will enable higher-confidence particle identification.

Acknowledgment

This work was performed under the auspices of the U.S. Department of Energy by University of California Lawrence Livermore National Laboratory under contract no. W-7405-ENG-48. This work is supported by the Lawrence Livermore National Laboratory through Laboratory Directed Research and Development grant No. 02-ERD-002. This project was funded in part by the Technical Support Working Group of the Department of Defense.

References

(1) Suess, D. T.; Prather, K. A. *Chem. Rev.* **1999**, *99*, 3007-3035.
(2) Johnston, M. V.; Wexler, A. S. *Anal. Chem.* **1995**, *67*, A721-A726.
(3) Murphy, D. M.; Thomson, D. S. *Aerosol Sci. Technol.* **1995**, *22*, 237-249.
(4) Hinz, K. P.; Kaufmann, R.; Spengler, B. *Anal. Chem.* **1994**, *66*, 2071-2076.
(5) Hinz, K. P.; Kaufmann, R.; Spengler, B. *Aerosol Sci. Technol.* **1996**, *24*, 233-242.
(6) Lazar, A.; Reilly, P. T. A.; Whitten, W. B.; Ramsey, J. M. *Environ. Sci. Technol.* **1999**, *33*, 3993-4001.
(7) Gard, E.; Mayer, J. E.; Morrical, B. D.; Dienes, T.; Fergenson, D. P.; Prather, K. A. *Anal. Chem.* **1997**, *69*, 4083-4091.
(8) Mallina, R. V.; Wexler, A. S.; Johnston, M. V. *J. Aerosol. Sci.* **1999**, *30*, 719-738.
(9) Salt, K.; Noble, C. A.; Prather, K. A. *Anal. Chem.* **1996**, *68*, 230-234.
(10) He, L.; Murray, K. K. *J. Mass Spectrom.* **1999**, *34*, 909-914.
(11) Jackson, S. N.; Murray, K. K. *Anal. Chem.* **2002**, *74*, 4841-4844.
(12) Stowers, M. A.; van Wuijckhuijse, A. L.; Marijnissen, J. C. M.; Scarlett, B.; van Baar, B. L. M.; Kientz, C. E. *Rapid Commun. Mass Spectrom.* **2000**, *14*, 829-833.
(13) Steele, P. T.; Tobias, H. J.; Fergenson, D. P.; Pitesky, M. E.; Horn, J. M.; Czerwieniec, G. A.; Russell, S. C.; Lebrilla, C. B.; Gard, E. E.; Frank, M. *Anal. Chem.* **2003**, *75*, 5480-5487.
(14) Hairston, P. P.; Ho, J.; Quant, F. R. *J. Aerosol. Sci.* **1997**, *28*, 471-482.
(15) Agranovski, V.; Ristovski, Z.; Hargreaves, M.; Blackall, P. J.; Morawska, L. *J. Aerosol. Sci.* **2003**, *34*, 301-317.
(16) Pan, Y. L.; Holler, S.; Chang, R. K.; Hill, S. C.; Pinnick, R. G.; Niles, S.; Bottiger, J. R. *Opt. Lett.* **1999**, *24*, 116-118.
(17) Kaye, P. H.; Barton, J. E.; Hirst, E.; Clark, J. M. *Appl. Optics* **2000**, *39*, 3738-3745.
(18) Eversole, J. D.; Cary, W. K.; Scotto, C. S.; Pierson, R.; Spence, M.; Campillo, A. J. *Field Anal. Chem. Technol.* **2001**, *5*, 205-212.
(19) Reyes, F. L.; Jeys, T. H.; Newbury, N. R.; Primmerman, C. A.; Rowe, G. S.; Sanchez, A. *Field Anal. Chem. Technol.* **1999**, *3*, 240-248.
(20) Hill, S. C.; Pinnick, R. G.; Niles, S.; Fell, N. F.; Pan, Y. L.; Bottiger, J.; Bronk, B. V.; Holler, S.; Chang, R. K. *Appl. Optics* **2001**, *40*, 3005-3013.
(21) Wenzel, R. J.; Prather, K. A. *Rapid Commun. Mass Spectrom.* **2004**, *18*, 1525-1533.
(22) May, K. R. *J. Aerosol. Sci.* **1973**, *4*, 235-243.
(23) Kinney, P. D.; Pui, D. Y. H.; Mulholland, G. W.; Bryner, N. P. *J. Res. Natl. Inst. Stand. Technol.* **1991**, *96*, 147-176.
(24) Auerbach, J. M.; Karpenko, V. P. *Appl. Optics* **1994**, *33*, 3179-3183.
(25) Hoffnagle, J. A.; Jefferson, C. M. *Appl. Optics* **2000**, *39*, 5488-5499.
(26) Ih, C. S. *Appl. Optics* **1972**, *11*, 694-695.
(27) Kanzler, K. *Proceedings of SPIE*, San Diego, CA 2001.
(28) Rohlfing, A.; Menzel, C.; Kukreja, L. M.; Hillenkamp, F.; Dreisewerd, K. *Journal of Physical Chemistry B* **2003**, *107*, 12275-12286.
(29) Dreisewerd, K.; Schurenberg, M.; Karas, M.; Hillenkamp, F. *Int. J. Mass Spectrom. Ion Process.* **1995**, *141*, 127-148.
(30) Srivastava, A.; Pitesky, M.; Steele, P.; Tobias, H.; Fergenson, D. P.; Horn, J.; Russell, S. C.; Czerwieniec, G.; Lebrilla, C.; Gard, E.; Frank, M. *Submitted for publication in Analytical Chemistry* **2004**.
(31) Czerwieniec, G. A.; Russell, S. C.; Tobias, H. J.; Fergenson, D. P.; Steele, P.; Pitesky, M. E.; Srivastava, A.; Horn, J. M.; Frank, M.; Gard, E. E.; Lebrilla, C. B. *Submitted for publication in Analytical Chemistry* **2005**.
(32) Tuminello, P. S.; Arakawa, E. T.; Khare, B. N.; Wrobel, J. M.; Querry, M. R.; Milham, M. E. *Appl. Optics* **1997**, *36*, 2818-2824.
(33) Mätzler, C. *MATLAB Functions for Mie Scattering and Absorption*, 2 ed.; University of Bern: Bern, Switzerland, 2002.

(34) Dean, D. H.; Douthit, H. A. *J. Bacteriol.* **1974**, *117*, 601-610.
(35) Fergenson, D. P.; Pitesky, M. E.; Tobias, H. J.; Steele, P. T.; Czerwieniec, G. A.; Russell, S. C.; Lebrilla, C. B.; Horn, J. M.; Coffee, K. R.; Srivastava, A.; Pillai, S. P.; Shih, M. T. P.; Hall, H. L.; Ramponi, A. J.; Chang, J. T.; Langlois, R. G.; Estacio, P. L.; Hadley, R. T.; Frank, M.; Gard, E. E. *Anal. Chem.* **2004**, *76*, 373-378.
(36) Gurton, K. P.; Ligon, D.; Kvavilashvili, R. *Appl. Optics* **2001**, *40*, 4443-4448.
(37) Griest, W. H.; Wise, M. B.; Hart, K. J.; Lammert, S. A.; Thompson, C. V.; Vass, A. A. *Field Anal. Chem. Technol.* **2001**, *5*, 177-184.
(38) Knochenmuss, R. *J. Mass Spectrom.* **2002**, *37*, 867-877.
(39) Campbell, S.; Beauchamp, J. L.; Rempe, M.; Lichtenberger, D. L. *Int. J. Mass Spectrom. Ion Process.* **1992**, *117*, 83-99.
(40) Stein, S. E.; Scott, D. R. *J. Am. Soc. Mass Spectrom.* **1994**, *5*, 859-866.

Figure Captions

Figure 1. The laboratory setup used to obtain dual-polarity mass spectra from individual Bacillus spores. Aerosolized spores are drawn into the instrument focused, tracked and then fired upon with the DI laser. Pulses from the DI laser pass through a series of optics to variably attenuate the pulse energy and to obtain a flattop profile.

Figure 2. Sample images show a) the "flat" profile (which looks the same at any energy), b) the low-fluence "Gaussian" profile and c) the high-fluence "Gaussian" profile. Each image is obtained from a single laser pulse. The maximum fluence in each image is scaled to one to enhance contrast. The true fluence distributions are shown in Figure 6.

Figure 3. Fluence "histograms" for flattop profiles with average pulse energies of (a) 222 mJ, (b) 155 mJ, (c) 119 mJ and (d) 71 mJ. In (a) the line represents the predicted result for a Gaussian profile with the same FWHM and pulse energy as the "flattop" profile (the fine structure results from pixelation). A true flattop would have all of its area contained in a single fluence bin.

Figure 4. Average B.at. spore (¼×TY) spectra collected using several different pulse energies. Note that the vertical range is different for different spectra and that both positive and negative ions are shown in each dual polarity spectrum.

Figure 5. The observed hit rates for B.at. spores (¼×TY) and the modeled hit rate curve based on a distribution of fluence thresholds with a mean of 1.0 nJ/μm^2 and a standard deviation of 0.23 nJ/μm^2.

Figure 6. Fluence distributions for (a) low-fluence flattop, (b) low-fluence Gaussian, (c) high-fluence flattop, and (d) high-fluence Gaussian. Care should be taken when comparing the vertical scales because

the histogram bins widths are not identical (this was necessary to avoid aliasing effects). The areas and the energies above the threshold (indicated by the gray line) are equal for the two low-fluence profiles and are also equal for the two high-fluence profiles.

Figure 7. Histograms of the normalized distances between individual spectra and the mean spectrum for (a) low-fluence flattop, (b) low-fluence Gaussian, (c) high-fluence flattop, and (d) high-fluence Gaussian. Tails of the distributions have been clipped for clarity. Larger distances indicate spectra more dissimilar to their mean. The RMS distances are labeled for each polarity of each set. The flattop data consistently shows less variability than the matching Gaussian data. Distances between negative ion vectors were assigned negative values for plotting.

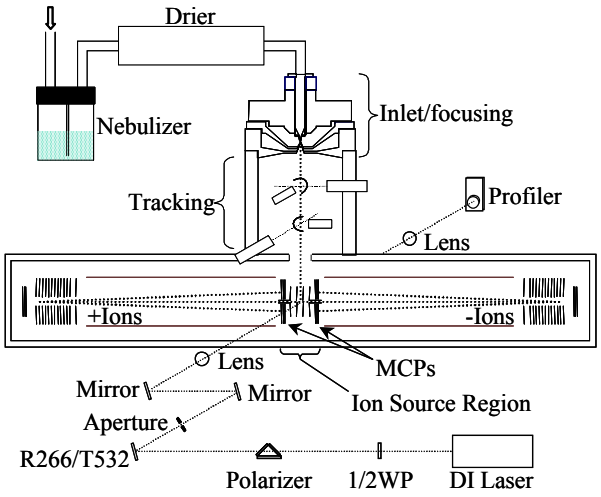

Figure 1. P. T. Steele, et. al.

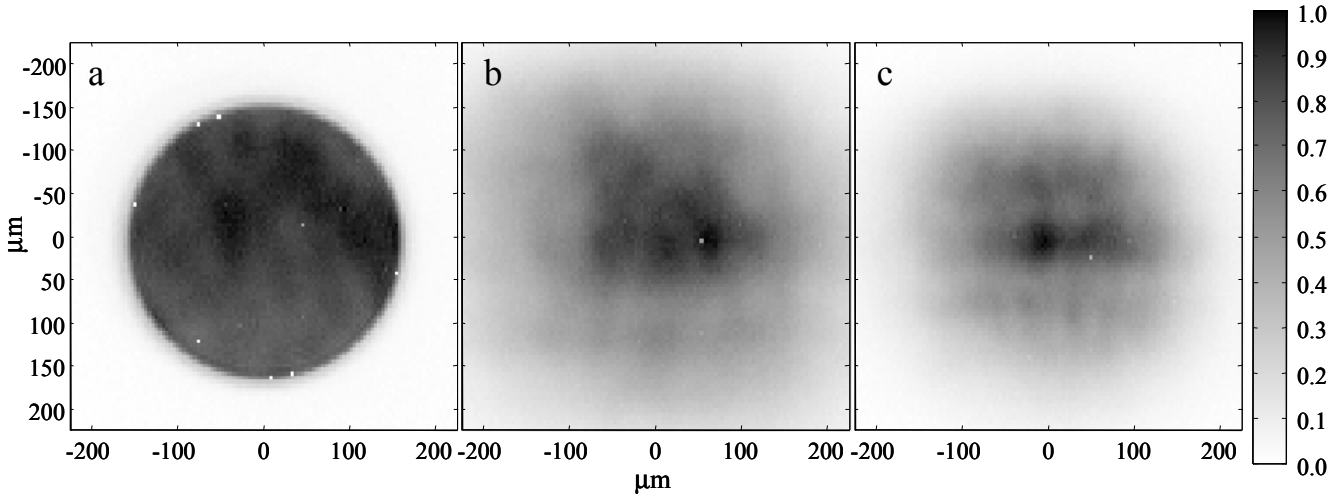

Figure 2. P. T. Steele, et. al.

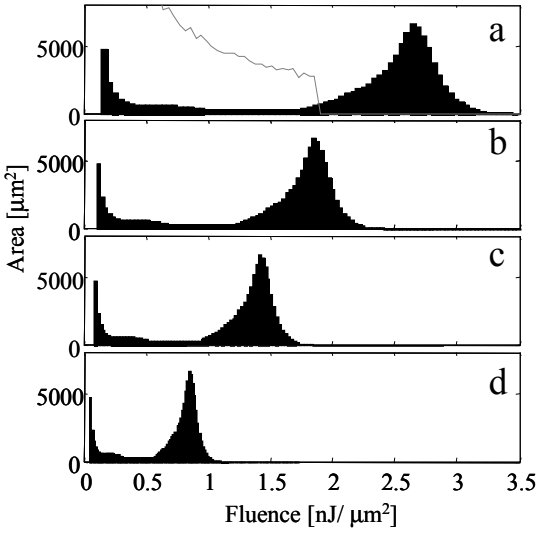

Figure 3. P. T. Steele, et. al.

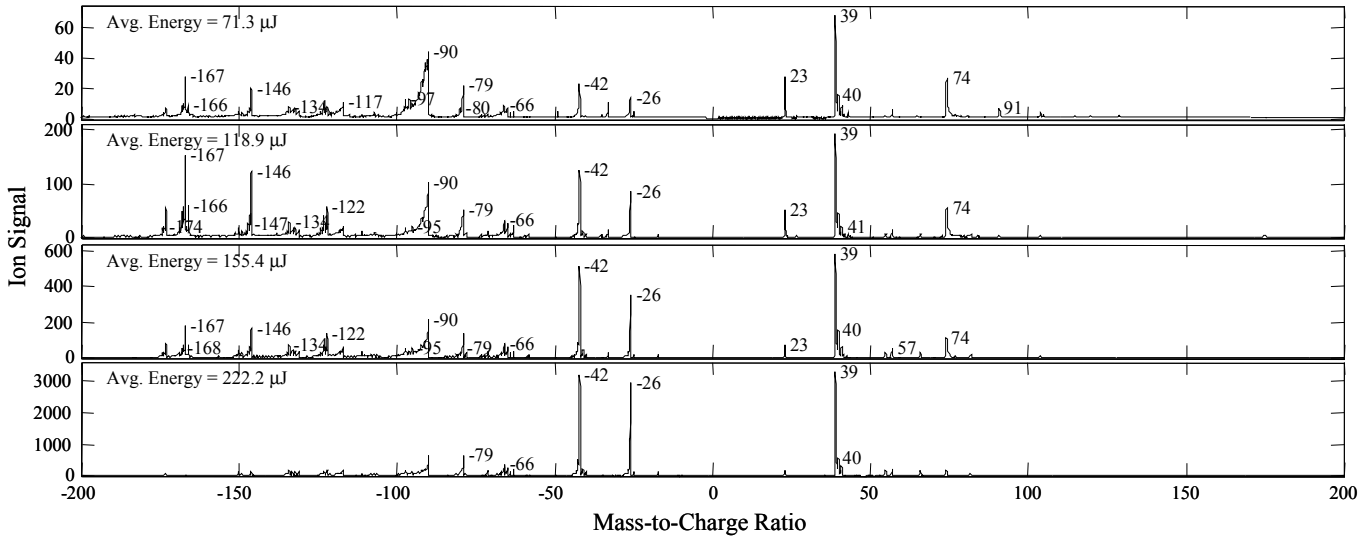

Figure 4. P. T. Steele, et. al.

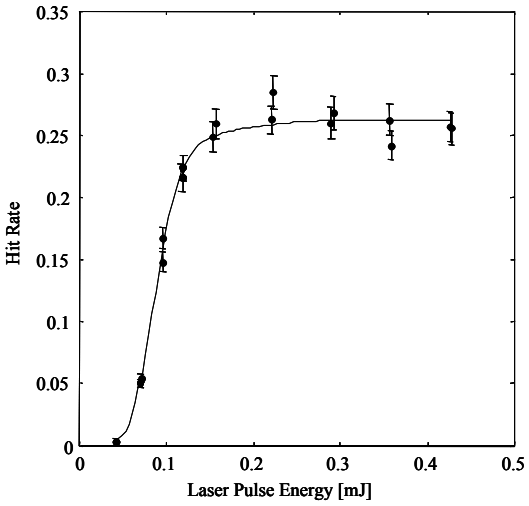

Figure 5. P. T. Steele, et. al.

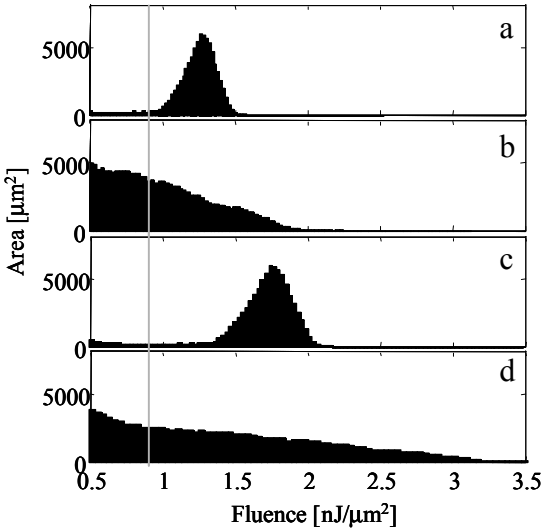

Figure 6. P. T. Steele, et. al.

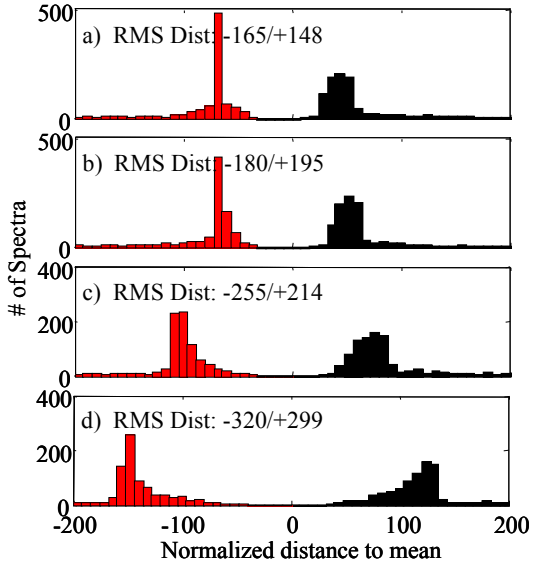

Figure 7. P. T. Steele, et. al.